Conference Proceedings

EuroSun 2016
Palma de Mallorca (Spain), 11 - 14 October 2016

Corrosion Behavior of Stainless Steel Alloys in Molten Solar Salt

A. Gomes[1], T. Paiva Luís[1], I. Figueira[1] and T.C. Diamantino[1]

[1] Laboratório Nacional de Energia e Geologia, Lisboa (Portugal)

Abstract

Molten nitrate salts ($NaNO_3$–KNO_3) have been widely used as heat transfer fluids (HTF) and energy storage media in concentrated solar power (CSP) plants. In the present work, the corrosion resistance of two austenitic stainless steels 316SS and 321SS was assessed during long term isothermal immersion in binary nitrate salt mixture, Solar Salt. The experiments were carried out at 550 °C under static conditions. The corrosion rates were determined by weight loss methodology, recording the weight changes of the coupons at different time intervals up to 3000 h. The corrosion scale products were characterized by scanning electron microscopy (SEM), energy-dispersive X-ray spectroscopy (EDS) and X-ray diffraction (XRD). The formation of multiple oxides was verified, being Fe_2O_3 and Fe_3O_4 the main products as confirmed by XRD. A stable $FeCr_2O_4$ inner layer was formed on the 316SS surface. At t>1000 h, a partial spallation occurred in the corrosion layers at 321SS. The corrosion rates were found to be 7.3 and 9.0 μm per year for 316SS and 321SS, respectively.

Keywords: *Molten nitrate salt, Heat transfer fluid, Thermal energy storage, Metallic corrosion*

1. Introduction

Thermal energy storage is a key performance parameter for improving the viability of the CSP plants. The accomplishment of this target allows the solar heat storage from solar radiation, to generate electricity at night or on overcast days with significant economic advantages of the solar plants. (Kuravi et al., 2013; Liu et al., 2016).

Nowadays, molten nitrate salts (MS) have been extensively used in CSP to transfer and store heat given their unique thermal properties (Vignarooban et al., 2015; Weinsten et al., 2015). In two-tank systems, based on MS as storage solution, the cold tank operates at 290 °C and the hot tank at temperatures greater than 550 °C. Due to the high operating temperature, the construction of the hot tank requires the use of stainless steel materials, being the austenitic stainless steels considered as prime candidates (Dorcheh et al., 2016).

At elevated temperatures, it was demonstrated that nitrate ions decompose giving rise to nitrite ions and oxygen (Nissen and Meeker, 1983). These strong oxidizing species combined with operating temperatures plus salt impurities generate propitious conditions for corrosion acceleration of stainless steels. In this context, it is crucial to evaluate the corrosion resistance and lifetime of stainless steels to optimize the material selection since their failure could lead to severe damage of the CSP plants operation.

In the present work, a comparative study of the corrosion resistance of two austenitic stainless steels, 316SS and 321SS, was assessed. The main objective was to evaluate the aging impact of the MS contact on the stability and corrosion properties of these container and piping materials, generally used in CSP, at the high-temperature at which the binary nitrate mixture (Solar Salt) is handled. To achieve this, static immersion tests have been performed, simulating the operative conditions in hot storage tanks at CSP plants.

The corrosion rates were determined by weight loss methodology, recording the weight changes of the coupons for long term isothermal immersion in Solar Salt (60% $NaNO_3$ and 40% KNO_3), for up to 3000 h at

© 2016. The Authors. Published by International Solar Energy Society
Selection and/or peer review under responsibility of Scientific Committee
doi:10.18086/eurosun.2016.03.12 Available at http://proceedings.ises.org

550 °C. The corrosion scale products were characterized by scanning electron microscopy, energy-dispersive X-ray spectroscopy and X-ray diffraction.

2. Experimental

Rectangular coupons measuring approximately 50 mm × 60 mm × 4 mm in thickness were cut from 316SS and 321SS stainless steel from Acerinox Europa and ACCIAITERNI (Italy), respectively. Table 1 shows the elemental composition of the studied stainless steels. Before corrosion tests, the coupons were ground with 320-grit SiC abrasive paper and then degreased by ethanol followed by rinsed with distillated water. After that the coupons were measured and weighted. Initial mass average values of (97.45±0.48) g for 316SS and (89.27±0.65) g for 321SS were recorded.

Tab. 1: Elemental composition of the studied stainless steels (wt.%)

Stainless steel	C	Mn	Si	P	Cr	Ni	Mo	Ti	Cu	Fe
316SS	0.020	1.346	0.361	0.036	16.635	10.025	2.011	–	–	Balanced
321SS	0.030	0.960	0.640	0.027	17.260	9.100	0.490	0.280	0.320	Balanced

The stainless steel coupons were mounted on sample hangers and fully immersed in binary nitrate molten salt mixture (60% $NaNO_3$ and 40% KNO_3). The nitrate salts were provided by SQM and COBRA and were used without further purification. The corrosion tests were performed at 550 °C with long-term duration up to 3000 h in presence of atmospheric air under static conditions. A vertical tubular furnace was used during this process. Four metallic samples were collected at different immersion intervals, namely 120, 1440 and 3000 h. After cooling at room temperature, the coupons were rinsed with distillated water and weighed after having been dried. Besides mass gain, descaling method was applied according to International Standard ISO 17245:2015 to evaluate the weight loss. From the descaled data, the corrosion rate (CR) was evaluated using equation 1 (Kruizenga and Gill, 2014)

$$CR\ (\mu m/yr) = \frac{87600\ \Delta m}{\rho\ t} \qquad \text{(eq. 1)}$$

where Δm is descaled mass loss per unit area (mg/cm^2), ρ is stainless steel density (g/cm^3) and t immersion time (hours).

To complement the stainless steel samples characterization, morphological and structural analysis were done before and after the corrosion process.

X-ray diffraction analysis of stainless steel coupons were carried out using a Rigaku Geigerflex D/MAX-III C diffractometer operating with a monochromatic Cu Kα radiation. XRD patterns were recorded in the 2θ range from 10 to 90°, using a 1.2º/min acquisition rate.

The elemental composition, surface and cross-sectional morphologies of the corrosion scale were investigated using a Phillips Scanning Electron Microscope, Model XL 30 FEG, coupled to an Energy Dispersive Spectrometer.

3. Results and discussion

The long-term corrosion process was evaluated through weight loss measurements as shown in Fig 1. Relatively low values of average weight loss were obtained. They increase with time, varying between 0.7 and 2.5 mg cm^{-2}. These results are acceptable for austenitic stainless steels under these experimental conditions and are similar to others reported by Kruizenga et al. (2013). After 3000 h of immersion, the corrosion rates were found to be 7.3 and 9.0 μm per year, at 550 °C, for 316SS and 321SS, respectively. The values obtained point to corrosion rate of 316SS is lower by 20% in comparison to 321SS. This suggests that

the corrosion scales formed in 316SS are slightly more protective than the ones formed in 321SS.

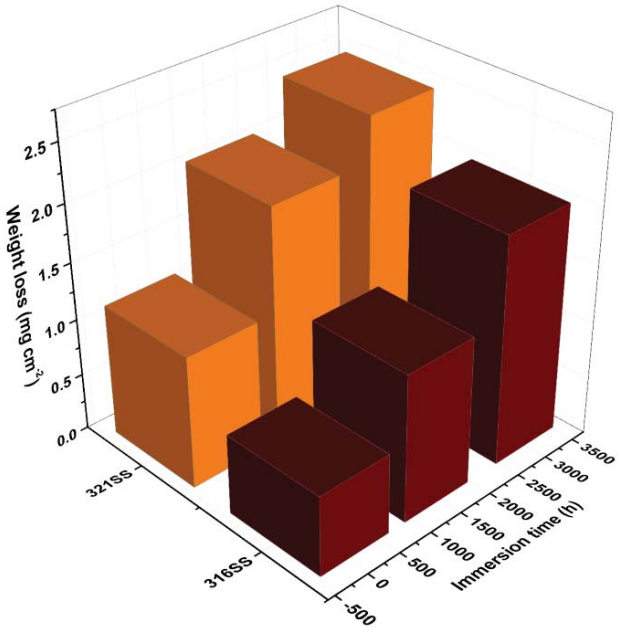

Fig. 1: Descaled weight loss data for 316SS and 321SS exposed to Solar Salt at 550 °C

After exposure to Solar Salt at 550 °C, corrosion products have been formed and the visual inspection of steel coupons shows that they lost their silver shiny aspect, acquiring a black colour for shorter times and a mixed black and rust-red coloration for longer times of immersion. By XRD analysis, it was depicted that the corrosion scale is composed of multiple crystalline oxide (Fe_2O_3, $FeCr_2O_4$, Fe_3O_4) compounds for both steel substrates, Fig 2. According to published studies, it could be assumed that Fe_2O_3 forms the external layer in contact with the molten salt, whereas Fe_3O_4 is located more internally near the metallic substrate (Fernández et al., 2012). Comparing the data recorded after 3000 h of exposure, it can be observed that the intensity ratio $I_{oxide\ scale}/I_{substrate}$ is higher for 316SS than for 321SS. This suggests that spallation phenomenon has occurred at the surface of 321SS for the longest immersion time. In addition, the XRD results pointed out that the relative abundance of iron oxides is different for the two stainless steels studied. Based on relative intensity of the diffraction peaks, it seems that the amount of spinel phases ($FeCr_2O_4$, Fe_3O_4) is more elevated at the 316SS surface. This may indicate that for 321SS, the surface protective Cr_2O_3 phase necessary to the formation of $FeCr_2O_4$ (see eq. 2) may be destroyed, promoting and accelerating the Fe corrosion due to the permeation of corrosion agents to the chromium depleted surface.

$$2\,Fe + 2\,Cr_2O_3 + O_2 \rightarrow 2\,FeCr_2O_4 \qquad \text{(eq. 2)}$$

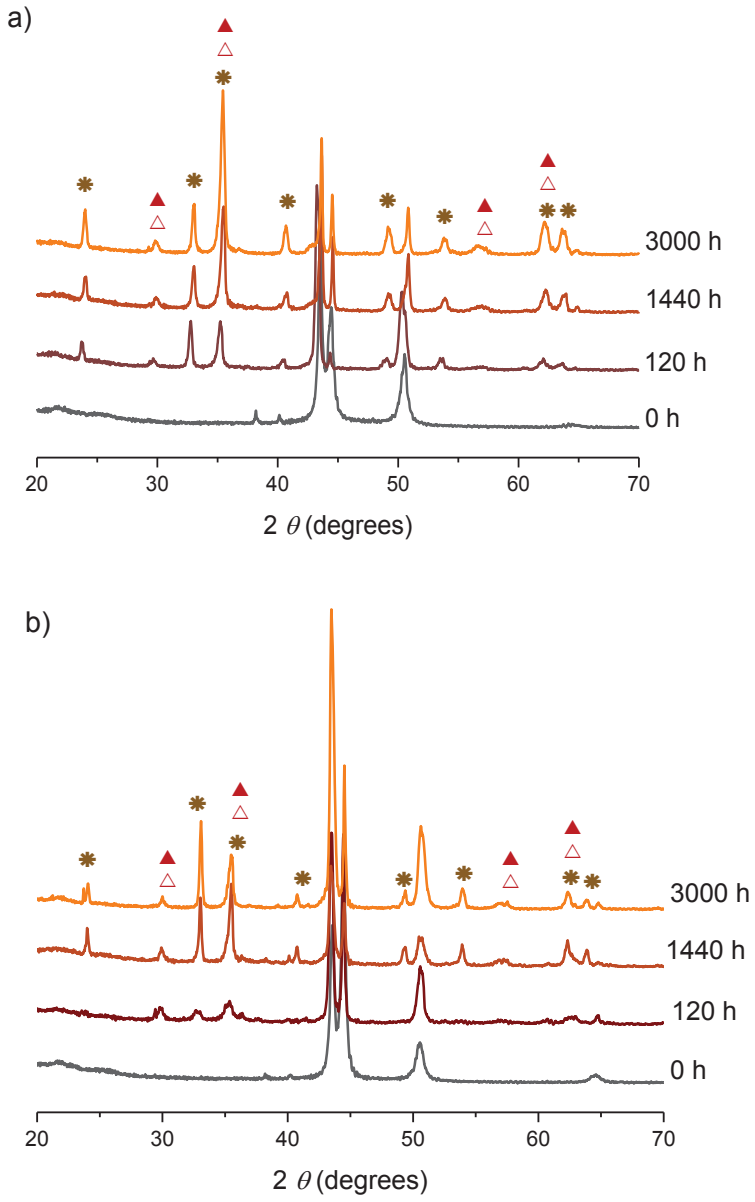

Fig. 2: XRD patterns of 316SS (a) and 321SS (b) immersed in Solar Salt for different time intervals (✱ - Fe_2O_3, △ - $FeCr_2O_4$, ▲ - Fe_3O_4)

Figures 3 and 4 show the morphological images of the surface of the oxide layers formed over time at the 316SS and 321SS, respectively. For comparison purposes, it is also shown the SEM image of the bare substrates where the abrasion marks can be easily observed. As it can be seen, after the oxidation process the surface of both steels became rougher and homogenously covered by an oxide layer. This is formed by polyhedral grains whose size increases with immersion time. At lower times, no cracks are observed at the oxide surface layer. However, partial surface spallation is observed on 321SS for exposure times equal or greater than 1440 h. This trend is not verified for the oxide scale formed at the 316SS, indicating that the scale corrosion is more adherent in this case. Spallation of oxide scales on stainless steel surfaces was previously reported (Trent et al., 2016), and explained due to stresses arising from the coefficient of thermal

expansion mismatch of the steel substrate and corrosion scale during cooling. In addition, the detachment of the oxide scales may also occur in –situ, leading to iron oxides re-growth (Scott and Wei, 1989).

From the cross-sectional images recorded after 3000 h of immersion, it is shown that the corrosion scales were multi-layered. For 316SS, a uniform and continuous inner layer was observed, and a less continuous and more irregular outer layer. According to this result, it seems plausible to assume that oxidation layers have been formed through uniform corrosion mode. For 321SS, it is evident that the oxide scale is detached from the substrate which is in agreement to other observations aforementioned. Furthermore, in this case it is more difficult to observe the irregular outer layer which could be related to mechanical failure during sample handling or metallographic preparation. Besides, in this sample, oxide features can also be seen just below the oxide-metal interface suggesting that oxide scale growth proceed via intergranular corrosion mode. More research is undertaken to better clarify the corrosion mechanism on both stainless steels.

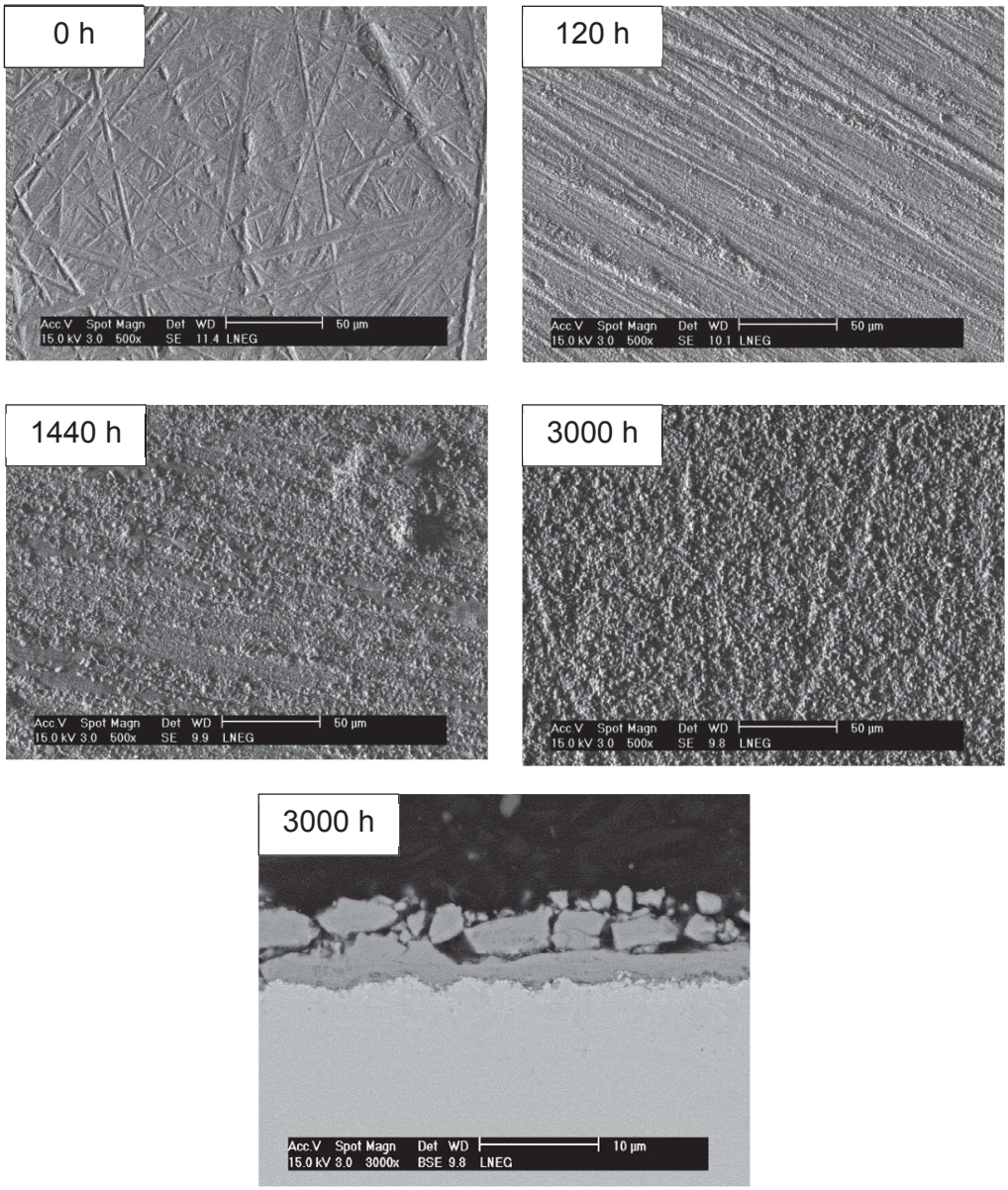

Fig. 3: Top view and cross-section SEM images of the oxide scales formed on 316SS after different immersion times in Solar Salt

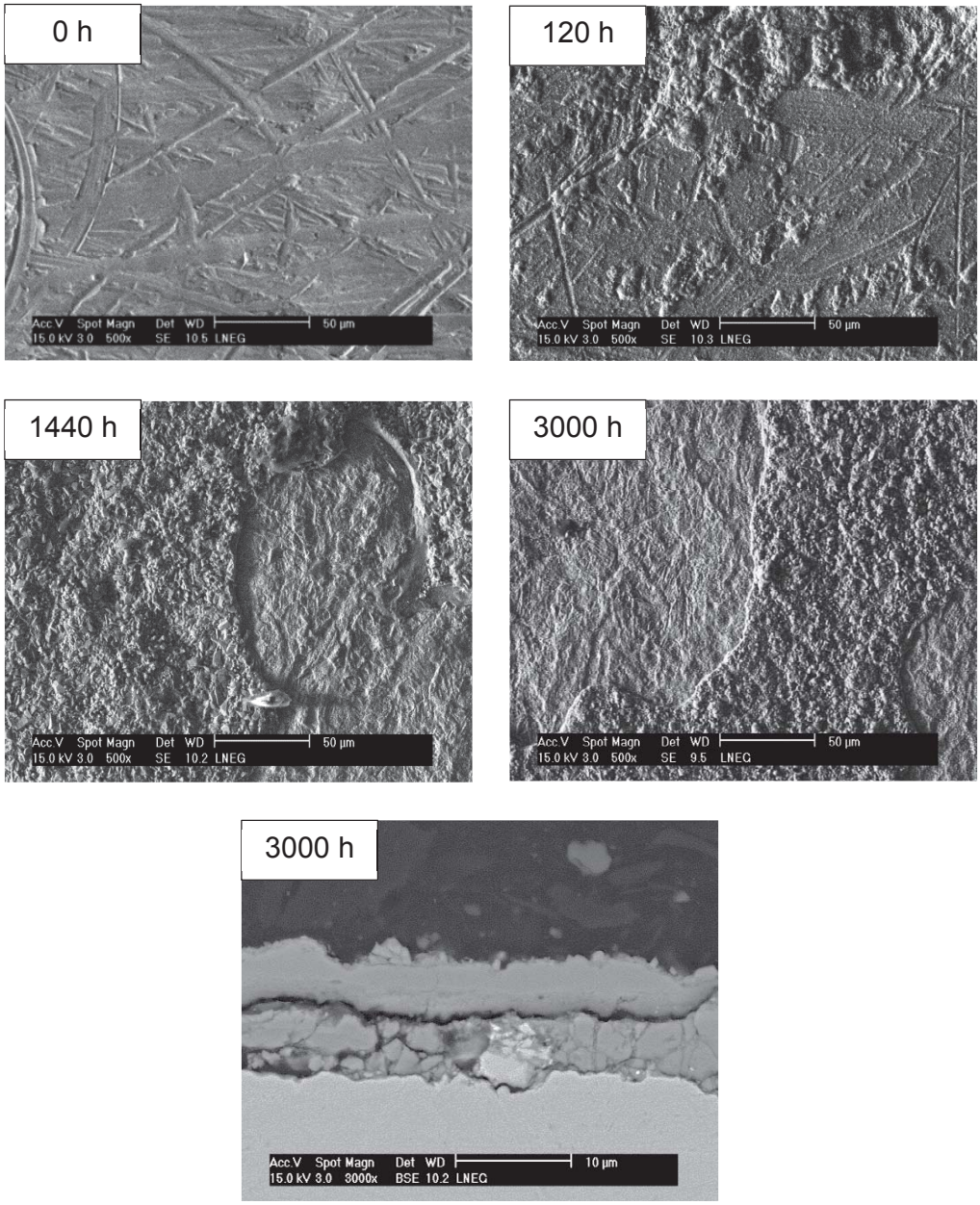

Fig. 4: Top view and cross-section SEM images of the oxide scales formed on 321SS after different immersion times in Solar Salt

Figure 5 show the elemental mapping of Cr, Ni, Fe and O for the corrosion scale developed after 3000 h of exposure for 316SS and 321SS, respectively. According to this figure, for both stainless steels, the outer layer of the corrosion scale is mainly composed by iron oxides. In the inner layer, an enrichment of chromium is verified. These results are in agreement with the XRD results. At the interface corrosion scale|steel substrate, nickel enrichment occurs, that is assumed to be the result of the depletion of chromium from the bulk (Kruizenga and Gill, 2014).

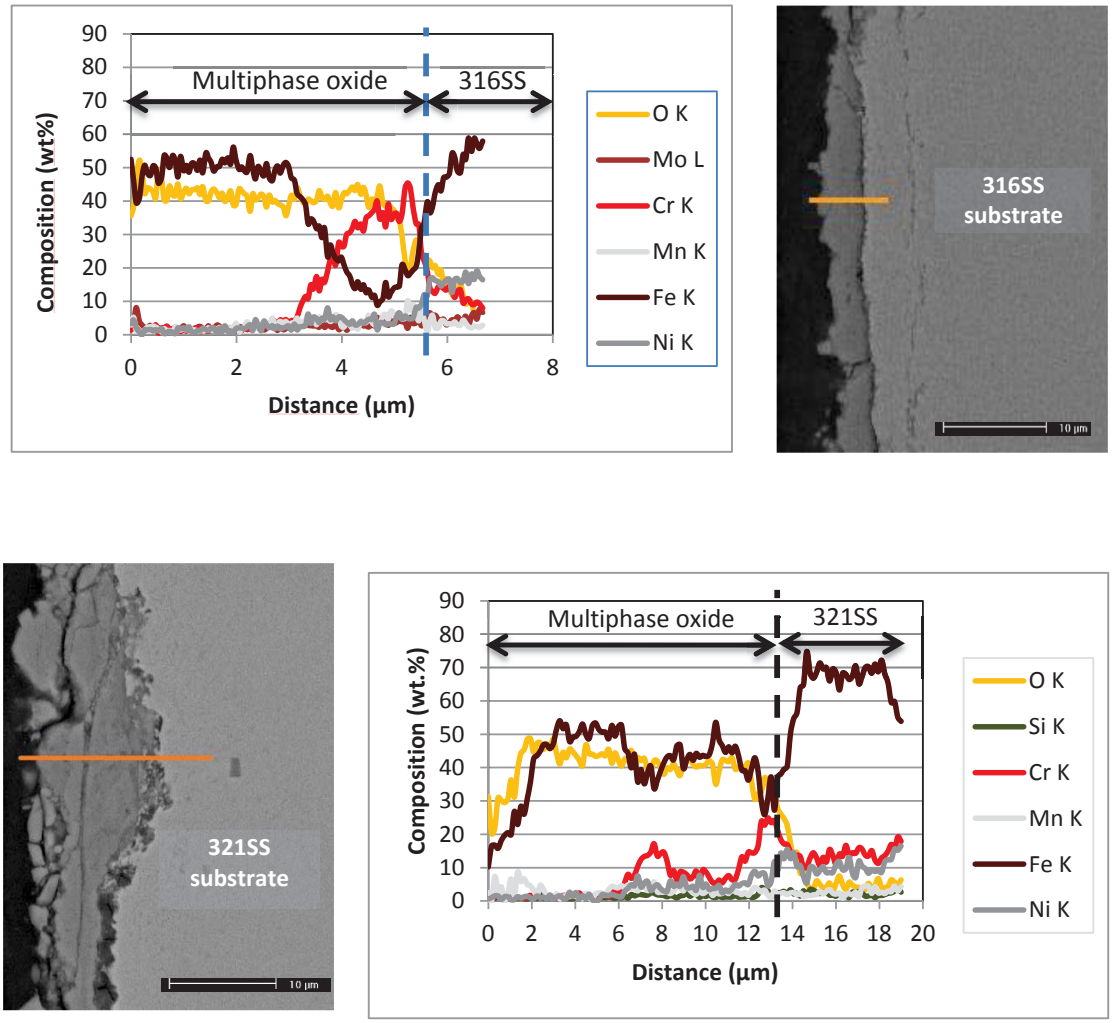

Fig. 5: Quantitative line scans and corresponding back scattered image of 316SS (a) and 321SS (b) after 3000 h immersed in MS

4. Conclusions

This study allows the following conclusions to be drawn:

- The formation of multiple oxides was verified, where Fe_2O_3 and Fe_3O_4 are the main corrosion products in both austenitic stainless steels.
- The scale morphology was similar for the two tested steel alloys.
- A stable $FeCr_2O_4$ inner layer was formed on 316SS surface.
- At t>1000 h, a partial spallation of the corrosion layers was observed at 321SS.
- After 3000 h of immersion, the corrosion rates were found to be 7.3 and 9.0 µm per year, at 550 °C, for 316SS and 321SS, respectively.

Further studies are underway to accurately determine the key factor that justifies the differences found on the corrosion behavior of these two austenitic materials.

Acknowledgments

The authors greatly appreciated the financial support from project STAGE-STE (http://www.stage-ste.eu/) Scientific and Technological Alliance for Guaranteeing the European Excellence in Concentrating Solar Thermal Energy, FP7 Grant Agreement 609837.

5. References

Dorcheh, A.S., Durham, R.N., Galetz, M.C., 2016. Corrosion behavior of stainless and low-chromium steels and IN625 in molten nitrate salts at 600 °C. Sol. Energ. Mat. Sol. C. 144, 109–116.

Fernández, A.G., Lasanta, M.I., Pérez, F.J., 2012. Molten salt corrosion of stainless steels and low-Cr steel in CSP plants. Oxid. Met. 78, 329–348.

ISO 17245: 2015 Corrosion of metals and alloys -- Test method for high temperature corrosion testing of metallic materials by immersing in molten salt or other liquids under static conditions.

Kruizenga, A., Gill, D., 2014. Corrosion of iron stainless steels in molten nitrate salt. Energy Procedia 49, 878 – 887.

Kruizenga, A.M., Gill, D.D., LaFord, M., McConohy, G., 2013. Corrosion of high temperature alloys in solar salt at 400, 500 and 680 °C. Albuquerque: Sandia National Laboratories. SAND2013-2526.

Kuravi, S., Trahan, J., Goswami, D.Y., Rahman, M.M., Stefanakos, E.K., 2013. Thermal energy storage technologies and systems for concentrating solar power plants. Prog. Energ. Combust. 39, 285-319.

Liu, M., Tay, N.H.S., Bell, S., Belusko, M., Jacob, R., Will, G., Saman, W., Bruno, F., 2016. Review on concentrating solar power plants and new developments in high temperature thermal energy storage technologies. Renew. Sust. Energ. Rev. 53, 1411–1432.

Nissen, D.A., Meeker, D.E., 1983. Nitrate/nitrite chemistry in $NaNO_3$-KNO_3 Melts. Inorg. Chem. 22, 716–721.

Scott, F.H., Wei, F.I., 1989. High temperature oxidation of commercial austenitic stainless steels. Mater. Sci. Tech. 5, 1140-1147.

Trent, M.C., Goods, S.H., Bradshaw, R.W., 2016. Comparison of corrosion performance of grade 316 and grade 347H stainless steels in molten nitrate salt. AIP Conf. Proc. 1734, 160017-1–160017-12.

Vignarooban, K., Xu, X., Arvay, A., Hsu, K., Kannan, A.M., 2015. Heat transfer fluids for concentrating solar power systems – A review. Appl. Energ. 146, 383–396.

Weinstein, L.A., Loomis, J., Bhatia, B., Bierman, D.M., Wang, E.N., Chen, G., 2015. Concentrating solar power. Chem. Rev. 115, 12797−12838.